ACS Energy LETTERS

http://pubs.acs.org/journal/aelccp

Structural and Interphasial Stabilities of Sulfurized Polyacrylonitrile (SPAN) Cathode

Sha Tan, Muhammad Mominur Rahman, Zhaohui Wu, Haodong Liu, Shen Wang, Sanjit Ghose, Hui Zhong, Iradwikanari Waluyo, Adrian Hunt, Ping Liu, Xiao-Qing Yang, and Enyuan Hu*

Cite This: *ACS Energy Lett.* 2023, 8, 2496−2504

Read Online

ACCESS | Metrics & More | Article Recommendations | Supporting Information

ABSTRACT: **Sulfurized polyacrylonitrile (SPAN) has attracted a lot of attention because of its low cost, high capacity, and great reversibility. Due to its structural complexity and amorphous nature, reaction mechanism of SPAN is little understood. Here we study the structural and interphasial changes of SPAN using synchrotron-based pair distribution function (PDF) analysis and soft X-ray absorption spectroscopy (sXAS). PDF identifies key structural features, including C−S bond, sulfur dimer, and sulfur chain in SPAN. The sulfur dimer bridging the pyridine network partially converts to sulfur chain during the first charging. In the following cycles, sulfur chain goes through lithiation and delithiation with reversibility dependent on the electrolytes. SXAS reveals surface changes of SPAN. After the first cycle, a negatively charged carbon or fused benzene layer is formed, on top of which is another layer formed by the electrolyte decomposition. The layer formed by localized high concentration electrolyte is stable during cycling.**

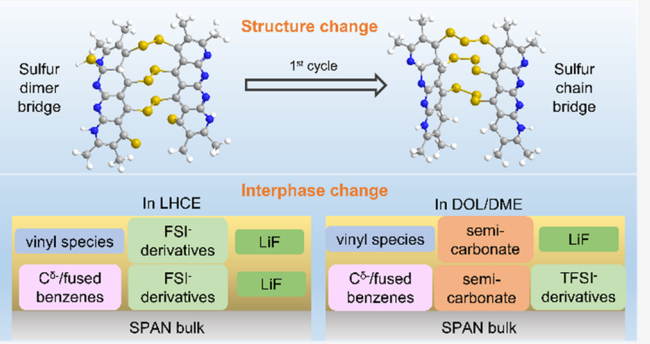

Lithium−sulfur (LillS) batteries are one of the most promising high energy density energy storage systems because it utilizes multielectron redox reaction and therefore delivers exceptionally large capacity.[1−4] Their cathodes are based on sulfur, which is cheap and abundant, having no reliance on the scarce and expensive transition metals that are needed by oxide cathodes. However, traditional LillS battery with elemental sulfur cathode faces stability issues owing to the polysulfide dissolution and the following shuttling effect, leading to active material loss, low Coulombic efficiency (CE) and short cycle life. To address these issues, an alternative cathode, sulfurized polyacrylonitrile (SPAN), has been extensively investigated. The SPAN cathode was first synthesized by Wang et al.[5] in 2002 by heating the sulfur and polyacrylonitrile (PAN) mixture under argon atmosphere. The obtained SPAN is more electronically conductive and delivers high capacity. More importantly, it can mitigate the polysulfide dissolution, providing a much more stable cycle life.

A lot of research efforts have been devoted to understanding the structure and charge storage mechanism of SPAN. Various characterization tools such as X-ray photoelectron spectroscopy (XPS), Raman spectroscopy, and nuclear magnetic resonance (NMR) were employed, and many reaction pathways have been proposed. Zhang et al. used thermogravimetric analysis, Raman and other elemental analysis techniques to characterize SPAN and proposed that the reversible breaking and reformation of S−S and C−S bonds are responsible for the capacity delivered.[6] Using NMR, electron paramagnetic resonance and simulation tools, Ming's group suggested that S−S bond breaking and reformation take place only in the first cycle, contributing to the capacity. For the following cycles, the capacity is from the reversible conversion between ionic SPAN and radical SPAN.[7] Recently, the combination of XPS, NMR, and Fourier transform infrared spectroscopy results suggest the breaking and reformation of N−S bond also contributes to the reversible lithium storage.[8] SPAN has considerable irreversible capacity loss in the first cycle. Its origin has been studied and understood as the irreversible reactions between lithium and C═C, C═N, or pyridine rings.[9] While these progresses have been made, there is still a lack of direct structural probe to answer some of the important questions facing SPAN. For example, are the changes of C−S and S−S bonds reversible? what is the linkage between sulfur atoms in the pristine material and how does that evolve during cycling?

Received: February 6, 2023
Accepted: May 1, 2023

https://doi.org/10.1021/acsenergylett.3c00281
ACS Energy Lett. 2023, 8, 2496−2504

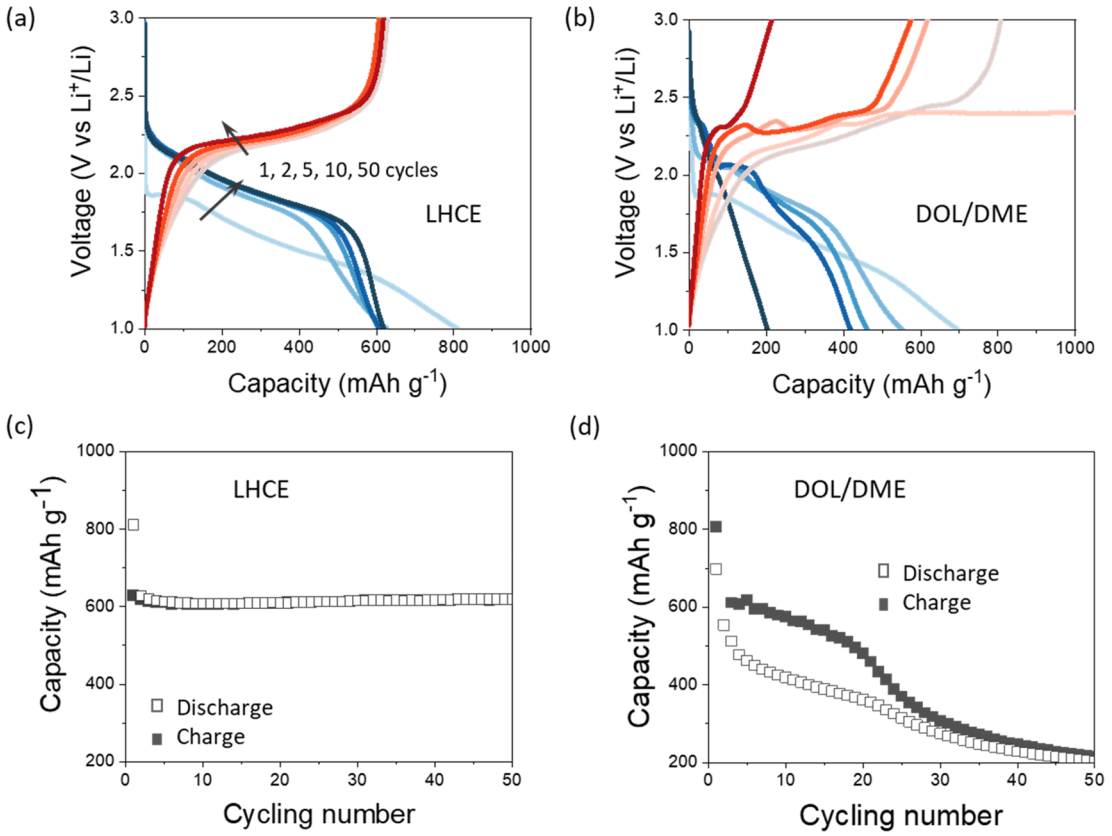

Figure 1. Charge−discharge profile of Li|SPAN battery using (a) LHCE and (b) DOL/DME electrolytes. The cycling performance of Li|SPAN using (c) LHCE and (d) DOL/DME electrolytes.

Much effort has also been devoted to improving the electrochemical performance of Li|SPAN system by optimizing the electrolyte.[10−12] Unlike the Li|S (elemental sulfur) system in which ether electrolyte is usually used, Li|SPAN typically employs carbonate electrolyte which is believed to be compatible with the SPAN cathode. However, the side reactions between carbonates and Li metal lead to stability issues. The widely used ether-based electrolytes in Li|S batteries are generally stable against lithium metal anode but suffer from problems of lithium polysulfides dissolution from the SPAN, resulting in capacity fading. Increasing salt concentration and introducing additives/cosolvents (i.e., fluoroethylene carbonate) can alleviate the shuttling effects.[13] Recently, localized high concentration electrolytes (LHCE) have been designed and used, showing efficient passivation of the lithium anode and suppression of the polysulfide dissolution.[14,15] To provide rational guidance of the electrolyte design, it is important to understand the interphase of SPAN in various electrolytes. Unfortunately, such information is very limited in the literature.

Herein, synchrotron-based techniques including X-ray pair distribution function (PDF) and soft X-ray absorption spectroscopy (sXAS) are utilized to characterize the structure and the interphase of SPAN. PDF is an ideal tool for analyzing complicated structures without crystallinity limitation and has been used for understanding polymer, interphase, as well as liquid systems.[16−18] SXAS probes the surface (1−100 nm) region of the sample and provides the chemical information. Using electron yield and fluorescence yield detection modes simultaneously, sXAS can differentiate the chemical information at different depths in the interphase.[19,20] We explore the structural and interphasial properties of SPAN and reveal how they are dependent on the electrolytes used for the Li|SPAN cells.

To investigate the structure and interphase of cycled SPAN cathode, two different electrolyte systems were studied, LHCE electrolyte (1.8 M LiFSI in DEE/BTFE; LiFSI, lithium bis(fluorosulfonyl)imide; DEE, diethyl ether; BTFE, bis-(2,2,2-trifluoroethyl)ether; weight ratio 1:4) and DOL/DME electrolyte (1 M LiTFSI in DOL/DME; LiTFSI, lithium bis(trifluoromethanesulfonyl)imide; DOL, 1,3-dioxolane; DME, 1,2-dimethoxyethane; volume ratio 1:1). The electrochemical results are displayed in Figure 1. When LHCE is used, the Li|SPAN battery shows a reversible charge and discharge behavior, maintaining a reversible capacity of ∼600 mAh g^{-1} during the first 50 cycles (Figure 1a). When DOL/DME electrolyte is used, there are plateaus at ∼2.1 V during discharge and at ∼2.4 V during charge. This may be due to the polysulfide shuttling effect as explained in previous SPAN studies by other research groups[6,10,21,22] (Figure 1b). Interestingly, the feature is different from the typical polysulfide shutting curve seen in Li−S batteries. A possible reason may be that the specific chemical nature of the polysulfides dissolved may be different (for example, the dissolved polysulfides may have different chain length for SPAN and for elemental sulfur) and the solvation process involved may also be different. The cycling stability is shown in Figure 1c,d, corresponding to LHCE and DOL/DME electrolyte, respectively. A stable capacity retention of ∼98.4% at the 50th cycle (based on the change capacity of the first cycle) was achieved when using LHCE electrolyte. In contrast, the Li|SPAN cell using DOL/DME electrolyte only

https://doi.org/10.1021/acsenergylett.3c00281
ACS Energy Lett. 2023, 8, 2496−2504

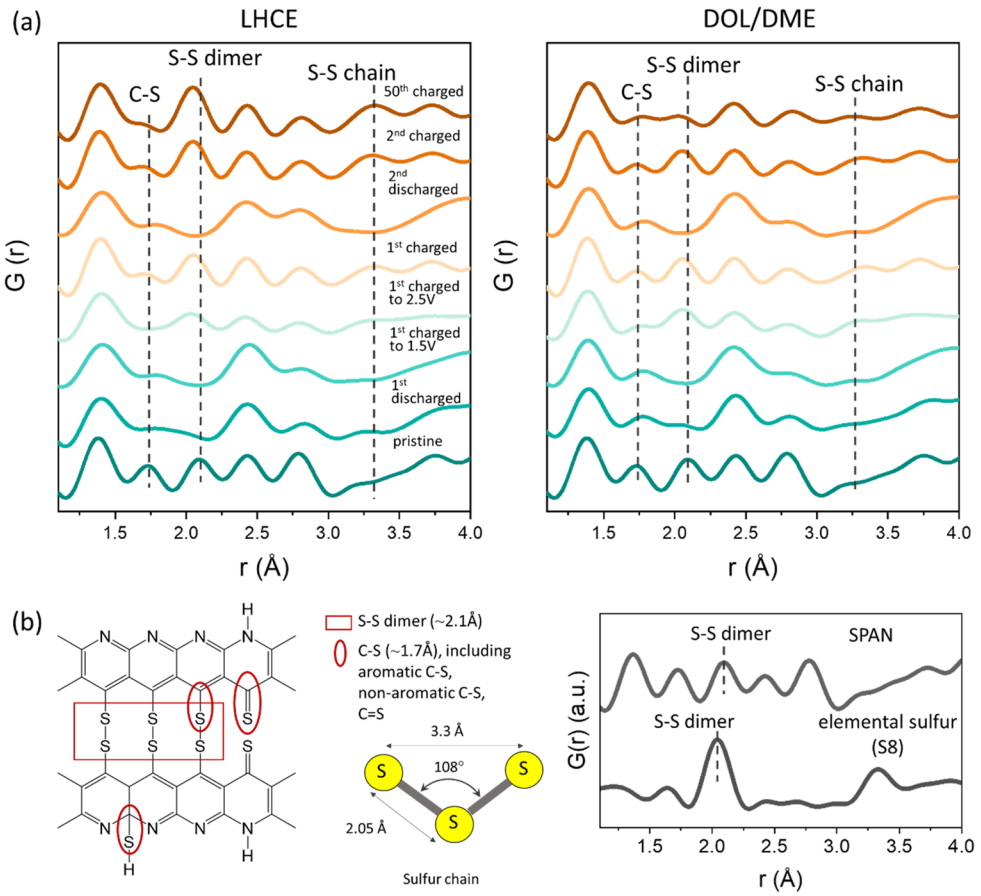

Figure 2. (a) PDF results of cycled SPAN cathode using LHCE and DOL/DME electrolytes. (b) (left) Molecular structure of SPAN and S−S interactions. (right) The PDF results of SPAN powder and elemental sulfur.

delivered a capacity of ~214 mAh g^{-1} at the 50th cycle, corresponding to a capacity retention of less than 30%. The distinct electrochemical performance suggests SPAN may experience different structural and interphasial evolution during cycling, which are systematically investigated and discussed below.

To understand the bulk structural change of SPAN, synchrotron-based PDF was utilized. It can monitor the evolution of bonds and interactions of atom pairs of interest during electrochemical cycling. In the pristine SPAN material, there are five peaks between 0.5 to 3.5 Å shown in the PDF results (Supporting Information (SI), Figure S1). Peaks 1, 4, and 5 correspond to the direct or indirect C−C/C−N interactions in the pyridine rings. Peaks 2 (at 1.73 Å) and 3 (at 2.10 Å) are very important for structural analysis as they correspond to C−S and S−S bonds in the SPAN structure, respectively, and do not overlap with peaks from other structural features.

Ex situ PDF results of pristine SPAN and cycled SPAN in LHCE and DOL/DME systems are shown in Figure 2a. In both LHCE and DOL/DME systems, C−S bond changes during cycling. The C−S bond length increases after discharge as indicated by the peak shifting to larger *r* values. This is likely caused by the lithiation process that leads to C−S−Li interaction. Upon charge, while the length of C−S bond decreases and mostly returns to the initial value in the pristine SPAN as indicated by the peak position change, the abundance of C−S bonds cannot be fully restored at the end of first cycle, as indicated by the peak intensity change. This suggests that some of the C−S bonds change into other chemical species and C−S bond may be associated with the irreversibility of the first cycle. The abundance of C−S bonds is further decreased upon cycling, as indicated by the peak intensity decrease. Combining this with the analysis of other structural changes, the loss of C−S bonds is likely associated with the sulfur dimer to sulfur chain conversion during cycling as will be elaborated later.

Another important structural feature is the S−S bond which is indicated by the PDF peak at 2.10 Å. In both electrolytes, the intensity of this peak decreases after first discharge, indicating the breaking of S−S bonds. This happens as SPAN is lithiated and lithium is attached to each sulfur belonging to the original S−S bond or the sulfur dimer. The intensity of the sulfur dimer peak gradually regains its intensity during charging, indicating the reformation of S−S bond. Interestingly, a new peak (at 3.3 Å) that is not present in the pristine SPAN appears after charging to 2.5 V. In the PDF data of elemental sulfur, it can be seen that the 3.3 Å peak arises from the presence of the second nearest-neighbor correlation among sulfur atoms (Figure 2b, and SI, Figure S2). As this structural feature appears only if sulfur chain is formed, the presence of the 3.3 Å peak is an effective indicator of sulfur chain formation. Its appearance indicates that during the first cycle, sulfur chains (−S−S−S−) which were not present in the pristine SPAN were formed upon electrochemical delithiation as illustrated in Figure 2b. It is worth noting that the development of sulfur chain peak is accompanied by the decrease of C−S peak, suggesting that sulfur from C−S bonds

https://doi.org/10.1021/acsenergylett.3c00281
ACS Energy Lett. 2023, 8, 2496−2504

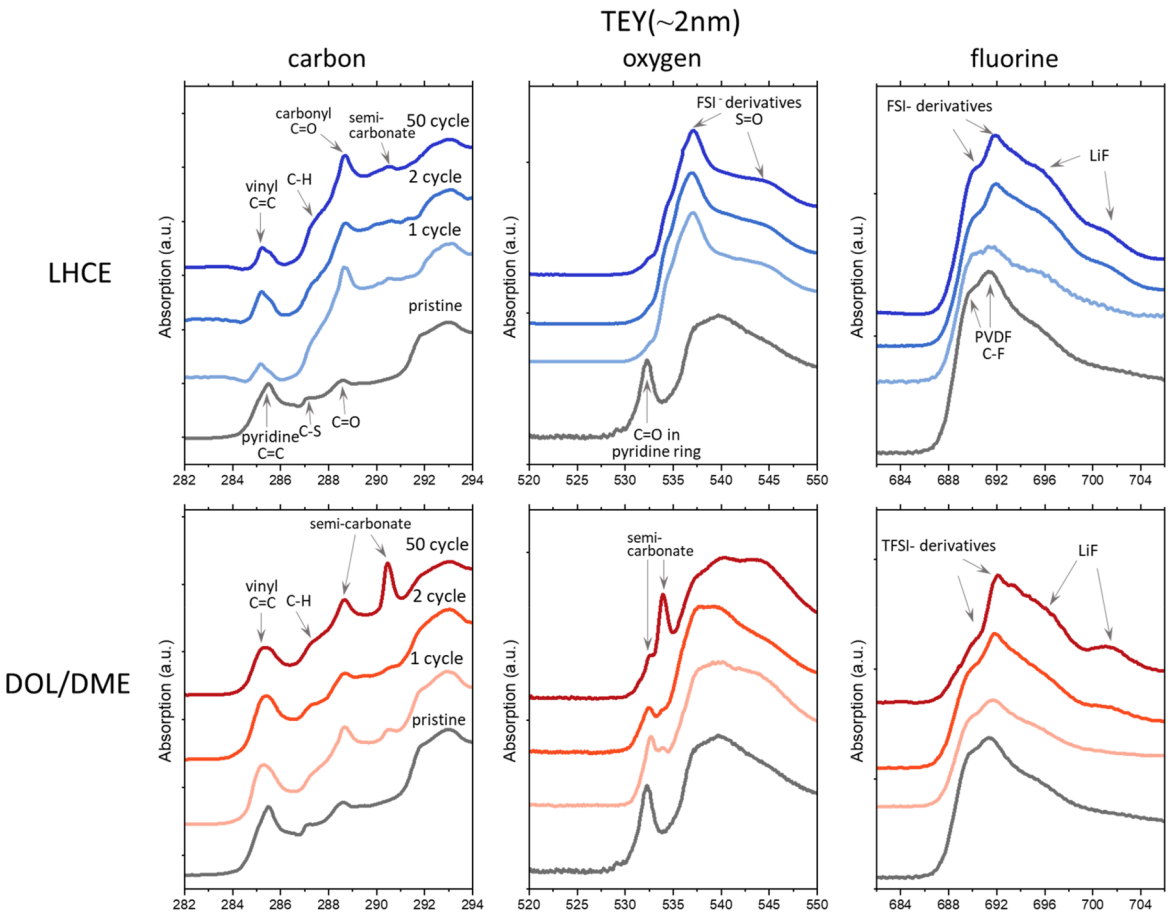

Figure 3. Carbon K-edge, oxygen K-edge, and fluorine K-edge soft XAS results of pristine and cycled SPAN in TEY mode after using LHCE (top) and DOL/DME (bottom) electrolytes.

(likely those nonaromatic C−S bond and C═S double bond) contributes to the formation of sulfur chain during cycling. The C═S and C−S bonds cannot be well distinguished by PDF data because their bond lengths are very close. However, the presence of C═S in the pristine SPAN can be identified by sulfur K-edge XAS as shown in our previous study.[21] It should be noted that while C═S bond has higher bond energy than the S−S bond, breaking of C═S bond and formation of S−S bond do not necessarily mean the net effect is an energy increase in the material. This is because formation of C═C bond which has high energy is very likely also involved during the process and the overall effect is a decrease in the energy of the SPAN. The right panel of Figure 2b shows the PDF data of SPAN and elemental sulfur, both in pristine state. It is clear that the S−S bond length in SPAN (the sulfur dimer connecting the pyridine networks) is longer than that in the elemental sulfur. This explains why the S−S bond shortens after sulfur chain formation as indicated by ex situ PDF data in Figure 2a. Previously, various pristine SPAN structures were proposed, including different S chain length and different bonding configurations (N−S_x−N or C−S_x−C).[23,24] Our PDF results in Figure 2b suggest the absence of sulfur chain in the pristine SPAN structure. Due to the fact that C−S and N−S have close bond lengths, the possibility of N−S bond cannot be validated or disapproved by PDF result. It should be noted that while conventional SPAN synthesis usually involve vacuum or Soxhlet extraction steps after obtaining SPAN powders from the furnace, we skipped these procedures out of the concern that they may remove some of the short chain sulfur and lead to reversible capacity loss. Intuitively, this may give rise to residual elemental sulfur which contains sulfur chains. However, the whole synthetic process is carried out in a tube furnace with Ar flow at the temperature of 450 °C. The excess sulfur, if there is any, would sublime and flow away from the products during the annealing process. That may explain the absence of long chain sulfur in the pristine SPAN material as indicated by the PDF results. These results also suggest that the structure of SPAN is highly dependent on the synthesis procedure.

In the first and second cycles, the behaviors of sulfur dimer and sulfur chain peaks are mostly the same between LHCE and DOL/DME electrolytes, suggesting the similar reaction mechanism in these two electrolytes. However, the behaviors of the two peaks are very different between the two electrolytes in the following cycles. For LHCE electrolyte, the peak intensity of S−S dimer remained almost unchanged during cycling, indicating sulfur inventory is well preserved. In contrast, for DOL/DME electrolyte, the intensities of S−S dimer peak gradually decreased after multiple cycling, suggesting the loss of sulfur. It is also noted that the peak intensity for the second-nearest-neighbor correlation S−S chain, which is an indication of short sulfur chains (−S−S−S−), experience similar evolution as the S−S dimer in these two electrolytes. For the LHCE electrolyte, the short sulfur chain is preserved during cycling. However, for the DOL/DME electrolyte, the loss of sulfur inventory leads to decrease

https://doi.org/10.1021/acsenergylett.3c00281
ACS Energy Lett. 2023, 8, 2496−2504

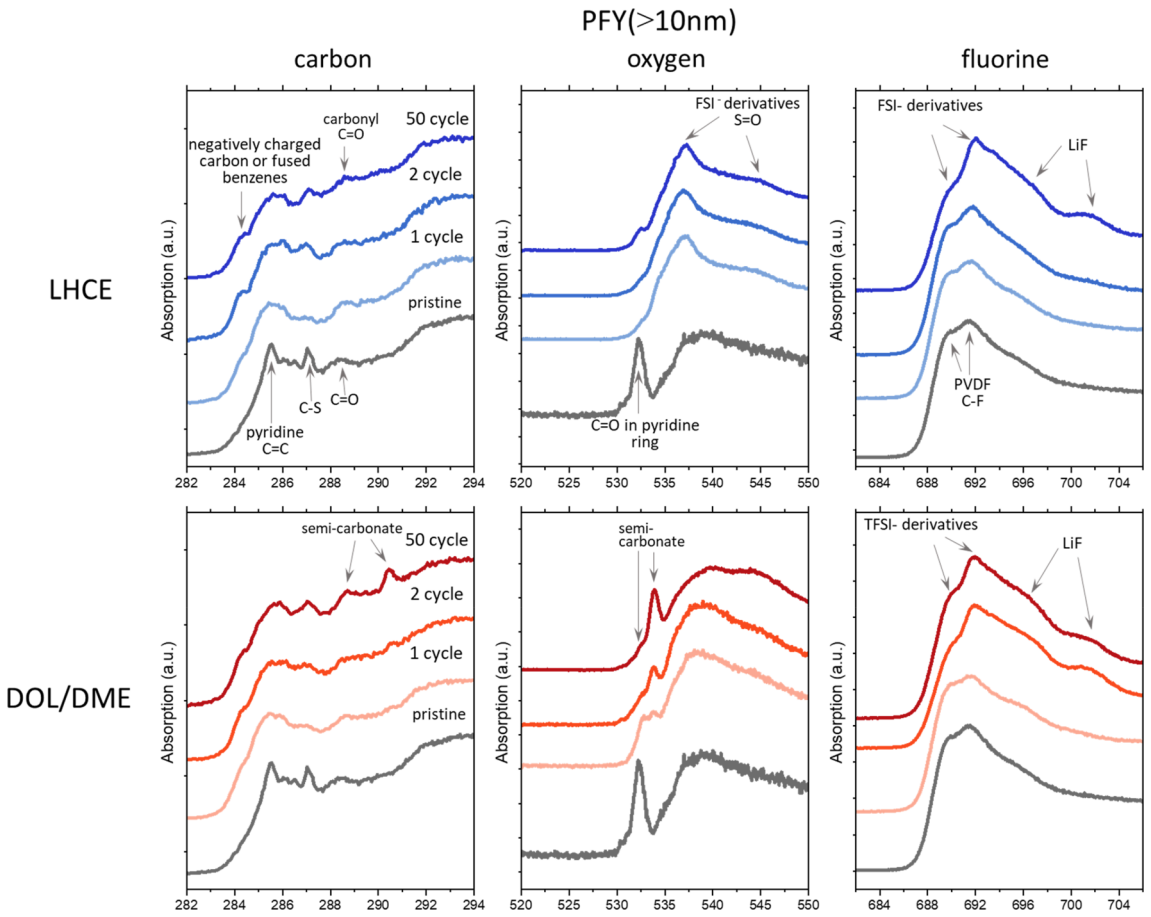

Figure 4. Carbon K-edge, oxygen K-edge, and fluorine K-edge soft XAS results of pristine and cycled SPAN in PFY mode after using LHCE (top) and DOL/DME (bottom) electrolytes.

in availabilities of both sulfur dimer and sulfur chain. The cause of sulfur loss in the DOL/DME electrolyte is likely the polysulfide dissolution. As shown in SI, Figure S3, the separator color changed from clear to yellow when the voltage reached to 2.5 V in the first cycle, which might be resulted from sulfur chain formation in SPAN followed by polysulfide dissolution in the electrolyte. In addition to C−S and S−S bonds, the peak at ∼2.8 Å, which corresponds to the longest interaction in the pyridine ring (SI, Figure S1), also changes during cycling. This is because the size of the ring changes in response to the lithiation/delithiation process. As a result, the atomic distance and the corresponding PDF peak position changes. The ring structures are in general uniform in the pristine SPAN but gradually lose the uniformity during cycling, leading to the PDF peak broadening and intensity decrease.

In addition to the bulk structure, the interphase is also important to the overall electrochemical performance. To study the interphase, *ex situ* sXAS was employed. The data was collected in both total electron yield (TEY) mode and partial fluorescence yield (PFY) mode which has probing depth of 2−5 nm and tens of nm, respectively. In the TEY mode (Figure 3), the results demonstrate the chemical information on the top cathode electrolyte interphase (CEI) on the cycled SPAN cathode. The evolution of carbon species is revealed in the carbon K-edge sXAS spectra. In the pristine sample, the peaks arise from different antibonding orbitals associated with the pyridine C═C, C−S, and C═O bonds,[25,26] which are labeled in Figure 3. After cycling, the pyridine C═C peak intensity decreased because of the CEI formation, and a vinyl C═C peak at lower energy was observed. Carbonyl and small amount of semicarbonates are also observed in the CEI formed in the LHCE electrolyte. When the DOL/DME electrolyte is used, the CEI is dominated by large amount of semicarbonates. This is probably due to the ring-opening and polymerization of DOL solvents.[27,28] Comparing among different cycles, LHCE forms a stable CEI even in the formation cycle as the spectra show little change from first cycle to the 50th cycle. However, the spectra collected from DOL/DME electrolyte keep evolving during cycling, suggesting continuous side reactions on the SPAN surface.

In the oxygen K-edge sXAS results, the pristine SPAN cathode has a single peak at ∼532 eV which might correspond to the C═O interactions on the pyridine ring. But it should be noted that oxygen amount in the pristine SPAN is very small as demonstrated by the very small edge jump shown in the raw sXAS data (SI, Figure S4), agreeing with the previous SPAN elemental analysis results.[10] Upon cycling, new peaks arise and evolve and their ways of evolution is highly dependent on the electrolyte used. In the LHCE electrolyte system, the salt anion (FSI^-) derived products are the dominant species, which is suggested by the sXAS of standard LiFSI material (SI, Figure S5). While in the DOL/DME electrolyte system, the sXAS spectra are dominated by the peaks corresponding to semicarbonate species, suggesting CEI is dominated by products resulting from DOL solvent decomposition. Comparing the spectra from different cycles, it is obvious that LHCE

https://doi.org/10.1021/acsenergylett.3c00281
ACS Energy Lett. 2023, 8, 2496−2504

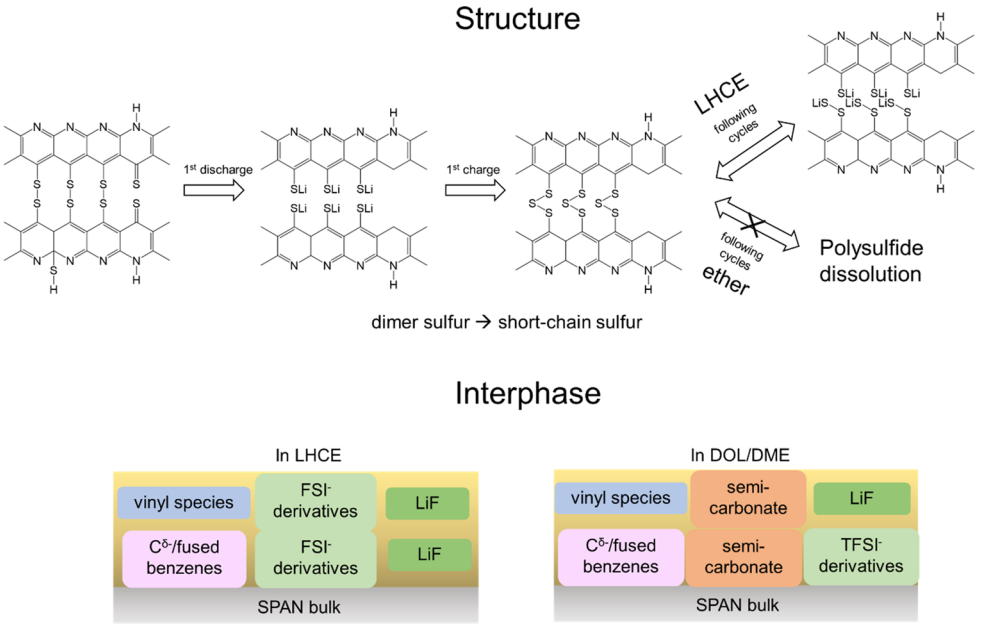

Figure 5. Schematic illustration of SPAN structural evolution (top) and interphasial development (bottom) during charging and discharging process.

generated much more stable interphase than DOL/DME electrolyte as the spectra of the former have little change during cycling.

The fluorine K-edge sXAS spectra show that for the pristine state, the signals are exclusively from the polyvinylidene fluoride (PVDF) binder which contains C−F bond. After the first cycle, there are additional peaks corresponding to FSI^- derived species in the spectra of SPAN cycled in LHCE electrolyte. In comparison, the spectra of SPAN cycled in DOL/DME electrolyte have little change after the first cycle, suggesting anion is not involved in the interphase formation. After 2 cycles, more peaks were observed owing to the fluorine-containing salt (either LiFSI salt in LHCE electrolyte or LiTFSI salt in DOL/DME electrolyte) or/and solvent decomposition during battery cycling. The fluorine sXAS spectra of LiFSI and LiTFSI salts are shown as references in SI, Figure S6. In the DOL/DME systems, the spectra kept evolving during cycling. After 50 cycles, the signals from PVDF in the initial cycles diminished and the spectra become dominated by $TFSI^-$ derivatives and LiF peaks, suggesting the formation of a LiF-rich CEI. In contrast, LHCE electrolyte enables a much more stable interphase formation, with the fluorine sXAS spectra showing minimum change after the second cycle. Its interphase is dominated by the LiF and FSI^- derived species.

The PFY results in Figure 4 provide the chemical information in the deeper CEI, with the possibility involving bulk SPAN cathode if the thickness of CEI is within the probing depth. It is reported that the nitrogen-rich, aromatic carbon backbone in the SPAN structure plays a significant role in enabling the highly reversible redox chemistry.[29] To gain more insights into this, C and N PFY spectra were collected for understanding the change of carbon and nitrogen in the structure after electrochemical cycling. In the carbon spectra, the different shape and peak in PFY and TEY modes suggest that the carbon species distribution has depth-dependence in the CEI. For example, the vinyl peaks are much weaker in PFY than those in TEY, indicating that these species are more likely on the top layer of CEI and on the side close to the electrolytes. Instead, negatively charged carbon or fused benzene signals are present in the PFY spectra, indicating they are in the bottom layer of CEI or are from the bulk SPAN, which experience changes after electrochemical cycling. Because most oxygen and fluorine species are from the electrolyte decomposition products which accumulate on the cathode surface, the TEY and PFY of oxygen and fluorine show similar peak shape and chemical information. Salt-derived species signals dominate the oxygen and fluorine spectra of cycled SPAN in LHCE electrolyte, while solvent and salt decomposition products both contribute to the CEI formed in the DOL/DME system. In detail, the peak intensities show some differences. For example, the TEY spectra of SPAN in DOL/DME electrolyte are dominated by LiF signals, but the PFY counterparts are dominated by peaks from $TFSI^-$ derived species with minor contributions from LiF. This change suggests a continuous salt decomposition and LiF accumulation at the surface of SPAN when DOL/DME electrolyte is used.

Nitrogen K-edge sXAS spectra have also been measured in both TEY and PFY modes. In the TEY mode (SI, Figure S7a), the N spectra of SPAN cycled in LHCE electrolyte is dominated by the FSI^- species. In the DOL/DME electrolyte system, the nitrogen signals are from both $TFSI^-$ and pristine SPAN. SI, Figure S7b, shows the PFY results for two electrolyte systems. In the pristine SPAN electrode, the pyridinic peak is observed, in agreement with the proposed structures in the previous literature.[30] After cycling, the pyridinic peak shoulders experienced some changes as marked in the shaded region. The higher energy shoulder (400−402 eV) disappears after first discharge but comes back after first charge. This reversible change is likely associated with the active role of nitrogen in the charge storage mechanism which has previously been reported.[31] In the lower energy region, the peaks experience some irreversible change for both LHCE and DOL/DME electrolytes, which is likely associated with the CEI formation process during cycling.

https://doi.org/10.1021/acsenergylett.3c00281
ACS Energy Lett. 2023, 8, 2496−2504

According to the sXAS results, the CEI formed in the LHCE electrolyte is dominated and stabilized by anion derived species including both molecule segments (likely amorphous) and LiF (likely crystalline). In contrast, the CEI formed in the DOL/DME electrolyte mainly consists of species from the continuous decomposition of salt and solvent. In comparison, we also studied the interphase of SPAN formed in the conventional carbonate electrolyte (1 M $LiPF_6$ in EC/EMC; EC, ethylene carbonate; EMC, ethyl methyl carbonate; weight ratio 3:7), which has been considered stable against SPAN cathode. The electrochemical performance and sXAS results are shown in SI, Figure S8 and S9, respectively. SI, Figure S8, shows that stable cycling of SPAN can be achieved using carbonate electrolyte in the first 50 cycles. In SI, Figure S9, there are semicarbonate species formed by the solvent decomposition and PF_6^- species accumulated on the SPAN surface during cycling. These results showed that carbonate electrolyte is not fully stable against SPAN cathode, and the side reactions lead to continuous electrolyte decomposition, may cause capacity decay after long-term cycling.

Based on the PDF and sXAS results, the evolution of the structure and the interphase are summarized in Figure 5. In the pristine SPAN structure, there are C−S bonds and sulfur dimers connecting the pyridine networks. After first discharge, lithiation breaks the S−S bond and forms the −S-Li entities, contributing to the electrochemical capacity. During the charge process, the SPAN structure undergoes structural change. The S−S dimer linking the pyridine rings is now replaced by the short sulfur chain (−S−S−S−). Such a process is accompanied by the breaking of nonaromatic C−S bond and C═S double bond, which supplies the sulfur atom needed in forming sulfur chains. The formed S−S chain is actively involved in the reversible lithiation and delithiation in the following cycles. In addition, the loss of sulfur inventory because of polysulfide dissolution in the DOL/DME electrolyte was observed. Soft XAS revealed the chemical composition and their distribution in the cycled SPAN surface. After cycling in both LHCE and DOL/DME electrolyte, vinyl species accumulate on the top CEI, while the negatively charged carbon or fused benzenes stay close to the bulk SPAN. The FSI^- derived interphase was formed in the LHCE, which was formed after the first/second cycle and highly stable, experiencing little change during cycling and effectively protecting SPAN cathode. Because of the compatibility between LHCE with both Li metal anode and SPAN cathode, the Li||SPAN battery delivers stable capacity when using LHCE electrolyte. However, in DOL/DME system, the unstable CEI generated by solvent and salt decomposition was not able to passivate SPAN cathode, resulting in polysulfide dissolution and rapid battery failure.

In this work, the structural and interphasial change of SPAN cathode in different electrolytes have been investigated. The synchrotron-based PDF monitored the C−S and S−S bond change during cycling. Sulfur dimers in the pristine SPAN convert into short sulfur chains upon electrochemical cycling, using sulfur atoms originally belonging to the C−S bond. When LHCE electrolyte is used, sulfur inventory is well maintained in SPAN and the short chain sulfur contributes to the capacity reversibly. However, in the case of DOL/DME electrolyte, polysulfide dissolution leads to sulfur loss from SPAN and the structure of SPAN cannot be maintained. The stability and chemical composition of the interphase on the cycled SPAN is highly dependent on the electrolyte. LHCE enables a stable and protective salt-derived CEI on the SPAN cathode, while the unstable interphase formed in DOL/DME and carbonate systems causes continuous solvent and salt decomposition. The utilization of PDF and sXAS not only provide new structural change mechanisms and comprehensive surface chemical information, but also serve as novel tools to investigate complicated and amorphous cathode system for further investigation.

Methods. Electrode and electrolyte preparation: The SPAN was synthesized by heating the mixture of elemental sulfur (Alfa Aesar) and polyacrylonitrile (Sigma-Aldrich, M_w = 150 000) in a weight ratio of 4:1 in an argon-flowing tube furnace at 450 °C for 6 h.[21] After cooling to room temperature, pristine SPAN with sulfur content of 43.03 wt % is obtained.[32] The SPAN cathode was prepared by mixing SPAN powder, conductive carbon, and polyvinylidene fluoride (PVDF) binder (weight ratio 8:1:1), with the addition of *N*-methyl-2-pyrrolidone (NMP) solvent. Afterward, the slurry was casted onto Al foil and then dried inside the vacuum oven at 80 °C overnight. The obtained electrodes were cut into 1/2" discs with a mass loading of 5 mg cm^{-2} for battery assembly.

Three different electrolytes, 1 M $LiPF_6$ in EC/EMC (3/7 wt %), 1 M LiTFSI in DOL/DME (1/1 vol %), and 1.8 M LiFSI in DEE/BTFE (1/4 wt %), were prepared in the glovebox with controlled oxygen and water level.

Electrochemical measurements: The 2032 type coin cells were used for the electrochemical performance evaluation. The Li||SPAN battery was assembled inside the glovebox using Li foil (thickness: 250 um) as anode and SPAN as cathode sandwiched by a Celgard 2320 separator. In each cell, 70 μL electrolyte was used. Galvanostatic cycling of Li||SPAN battery was conducted within the voltage range of 1−3 V at a current density of 0.1 A g^{-1}.

Synchrotron characterizations: The cycled SPAN cathode after certain cycles was collected, washed by electrolyte solvent, and then dried for advanced characterizations. For PDF characterizations, the SPAN powder was collected from the cycled electrode using doctor blade. Then the powder samples were packed inside the capillary sealed by epoxy to avoid air contamination. The PDF measurements were carried out at the 28-ID-2 (XPD) beamline of National Synchrotron Light Source II (NSLS-II) at Brookhaven National Laboratory (BNL), using a photon wavelength of 0.18475 Å. Each sample was measured for 20 min to obtain a high-quality data. The obtained data was integrated using Fit2D software.[33] The PDF and G(r) values were extracted using PDFgetX3 software.[34] For sXAS characterizations, the SPAN cathode was cut into 2 × 5 mm^2 pieces and attached to the sample holder using copper tape before it was loaded into the vacuum endstation. The sXAS experiments were performed at the 23-ID-2 (IOS) beamline of NSLS-II at BNL. Both TEY (drain current) and PFY (Vortex EM detector) signals were collected at the carbon, nitrogen, oxygen, and fluorine K-edges. The obtained XAS results were analyzed using the Athena software package.[35]

■ ASSOCIATED CONTENT

Supporting Information

The Supporting Information is available free of charge at https://pubs.acs.org/doi/10.1021/acsenergylett.3c00281.

PDF results of SPAN and reference materials; optical images of cycled separators; raw soft XAS spectra of O K-edge at PFY mode; LiFSI and LiTFSI reference

https://doi.org/10.1021/acsenergylett.3c00281
ACS Energy Lett. 2023, 8, 2496−2504

spectra; nitrogen K-edge spectra at TEY and PFY mode; cycling performance of Li||SPAN using carbonate electrolyte; sXAS results of cycled SPAN collected in carbonate electrolyte (PDF)

AUTHOR INFORMATION

Corresponding Author

Enyuan Hu − *Chemistry Division, Brookhaven National Laboratory, Upton, New York 11973, United States;* orcid.org/0000-0002-1881-4534; Email: enhu@bnl.gov

Authors

Sha Tan − *Chemistry Division, Brookhaven National Laboratory, Upton, New York 11973, United States;* orcid.org/0000-0001-8277-893X

Muhammad Mominur Rahman − *Chemistry Division, Brookhaven National Laboratory, Upton, New York 11973, United States*

Zhaohui Wu − *Department of Nano Engineering, University of California San Diego, La Jolla, California 92093, United States*

Haodong Liu − *Department of Nano Engineering, University of California San Diego, La Jolla, California 92093, United States*

Shen Wang − *Department of Nano Engineering, University of California San Diego, La Jolla, California 92093, United States*

Sanjit Ghose − *National Synchrotron Light Source II, Brookhaven National Laboratory, Upton, New York 11973, United States*

Hui Zhong − *Department of Joint Photon Sciences Institute, Stony Brook University, Stony Brook, New York 11790, United States*

Iradwikanari Waluyo − *National Synchrotron Light Source II, Brookhaven National Laboratory, Upton, New York 11973, United States;* orcid.org/0000-0002-4046-9722

Adrian Hunt − *National Synchrotron Light Source II, Brookhaven National Laboratory, Upton, New York 11973, United States;* orcid.org/0000-0002-5283-9647

Ping Liu − *Department of Nano Engineering, University of California San Diego, La Jolla, California 92093, United States;* orcid.org/0000-0002-1488-1668

Xiao-Qing Yang − *Chemistry Division, Brookhaven National Laboratory, Upton, New York 11973, United States;* orcid.org/0000-0002-3625-3478

Complete contact information is available at: https://pubs.acs.org/10.1021/acsenergylett.3c00281

Notes

The authors declare no competing financial interest.

ACKNOWLEDGMENTS

The work at Brookhaven National Laboratory is supported by the Assistant Secretary for Energy Efficiency and Renewable Energy, Vehicle Technology Office, of the US Department of Energy (DOE) through the Advanced Battery Materials Research (BMR) Program including the Battery500 Consortium under contract no. DE-SC0012704. The same program also supports the work at UC San Diego through the Pacific Northwest National Laboratory under contract no. PNNL-595241. This research used 28-ID-2 (XPD) and 23-ID-2 (IOS) beamlines of the National Synchrotron Light Source II, U.S. DOE Office of Science User Facilities, operated for the DOE Office of Science by Brookhaven National Laboratory under contract no. DE-SC0012704.

REFERENCES

(1) Manthiram, A.; Fu, Y.; Chung, S.-H.; Zu, C.; Su, Y.-S. Rechargeable Lithium−Sulfur Batteries. *Chem. Rev.* **2014**, *114* (23), 11751−11787.

(2) Shadike, Z.; Tan, S.; Wang, Q.-C.; Lin, R.; Hu, E.; Qu, D.; Yang, X.-Q. Review on organosulfur materials for rechargeable lithium batteries. *Mater. Horiz.* **2021**, *8* (2), 471−500.

(3) Yin, Y.-X.; Xin, S.; Guo, Y.-G.; Wan, L.-J. Lithium−Sulfur Batteries: Electrochemistry, Materials, and Prospects. *Angew. Chem., Int. Ed.* **2013**, *52* (50), 13186−13200.

(4) Wu, Y.; Xie, L.; Ming, H.; Guo, Y.; Hwang, J.-Y.; Wang, W.; He, X.; Wang, L.; Alshareef, H. N.; Sun, Y.-K.; et al. An Empirical Model for the Design of Batteries with High Energy Density. *ACS Energy Lett.* **2020**, *5* (3), 807−816.

(5) Wang, J.; Yang, J.; Xie, J.; Xu, N. A Novel Conductive Polymer−Sulfur Composite Cathode Material for Rechargeable Lithium Batteries. *Adv. Mater.* **2002**, *14* (13−14), 963−965.

(6) Zhang, S. S. Understanding of Sulfurized Polyacrylonitrile for Superior Performance Lithium/Sulfur Battery. *Energies* **2014**, *7* (7), 4588−4600.

(7) Wang, W.; Cao, Z.; Elia, G. A.; Wu, Y.; Wahyudi, W.; Abou-Hamad, E.; Emwas, A.-H.; Cavallo, L.; Li, L.-J.; Ming, J. Recognizing the Mechanism of Sulfurized Polyacrylonitrile Cathode Materials for Li−S Batteries and beyond in Al−S Batteries. *ACS Energy Lett.* **2018**, *3* (12), 2899−2907.

(8) Weret, M. A.; Jeffrey Kuo, C.-F.; Zeleke, T. S.; Beyene, T. T.; Tsai, M.-C.; Huang, C.-J.; Berhe, G. B.; Su, W.-N.; Hwang, B.-J. Mechanistic understanding of the Sulfurized-Poly(acrylonitrile) cathode for lithium-sulfur batteries. *Energy Storage Mater.* **2020**, *26*, 483−493.

(9) Zhao, X.; Wang, C.; Li, Z.; Hu, X.; Abdul Razzaq, A.; Deng, Z. Sulfurized polyacrylonitrile for high-performance lithium sulfur batteries: advances and prospects. *J. Mater. Chem. A* **2021**, *9* (35), 19282−19297.

(10) Xing, X.; Li, Y.; Wang, X.; Petrova, V.; Liu, H.; Liu, P. Cathode electrolyte interface enabling stable Li−S batteries. *Energy Storage Mater.* **2019**, *21*, 474−480.

(11) Fanous, J.; Wegner, M.; Grimminger, J.; Andresen, Ä.; Buchmeiser, M. R. Structure-Related Electrochemistry of Sulfur-Poly(acrylonitrile) Composite Cathode Materials for Rechargeable Lithium Batteries. *Chem. Mater.* **2011**, *23* (22), 5024−5028.

(12) He, Y.; Zou, P.; Bak, S.-M.; Wang, C.; Zhang, R.; Yao, L.; Du, Y.; Hu, E.; Lin, R.; Xin, H. L. Dual Passivation of Cathode and Anode through Electrode−Electrolyte Interface Engineering Enables Long-Lifespan Li Metal−SPAN Batteries. *ACS Energy Lett.* **2022**, *7* (9), 2866−2875.

(13) Frey, M.; Zenn, R. K.; Warneke, S.; Müller, K.; Hintennach, A.; Dinnebier, R. E.; Buchmeiser, M. R. Easily Accessible, Textile Fiber-Based Sulfurized Poly(acrylonitrile) as Li/S Cathode Material: Correlating Electrochemical Performance with Morphology and Structure. *ACS Energy Lett.* **2017**, *2* (3), 595−604.

(14) Liu, H.; Holoubek, J.; Zhou, H.; Chen, A.; Chang, N.; Wu, Z.; Yu, S.; Yan, Q.; Xing, X.; Li, Y.; et al. Ultrahigh coulombic efficiency electrolyte enables Li||SPAN batteries with superior cycling performance. *Mater. Today* **2021**, *42*, 17−28.

(15) Wu, Z.; Liu, H.; Holoubek, J.; Anderson, C.; Shi, L.; Khemchandani, H.; Lu, D.; Liu, D.; Niu, C.; Xiao, J.; et al. The Role of Ion Transport in the Failure of High Areal Capacity Li Metal Batteries. *ACS Energy Lett.* **2022**, *7* (8), 2701−2710.

(16) Wang, X.; Tan, S.; Yang, X.-Q.; Hu, E. Pair distribution function analysis: Fundamentals and application to battery materials. *Chin. Phys. B* **2020**, *29* (2), 028802.

(17) Luo, C.; Hu, E.; Gaskell, K. J.; Fan, X.; Gao, T.; Cui, C.; Ghose, S.; Yang, X.-Q.; Wang, C. A chemically stabilized sulfur cathode for

lean electrolyte lithium sulfur batteries. *Proc. Natl. Acad. Sci. U.S.A.* **2020**, *117* (26), 14712−14720.
(18) Shadike, Z.; Lee, H.; Borodin, O.; Cao, X.; Fan, X.; Wang, X.; Lin, R.; Bak, S.-M.; Ghose, S.; Xu, K.; et al. Identification of LiH and nanocrystalline LiF in the solid−electrolyte interphase of lithium metal anodes. *Nat. Nanotechnol.* **2021**, *16* (5), 549−554.
(19) Wu, B.; Wang, B.; Petit, T. Soft X-ray spectroscopy of light elements in energy storage materials. *Energy Storage Mater.* **2021**, *40*, 72−95.
(20) Deng, J.; Zhang, Q.; Lv, X.; Zhang, D.; Xu, H.; Ma, D.; Zhong, J. Understanding Photoelectrochemical Water Oxidation with X-ray Absorption Spectroscopy. *ACS Energy Lett.* **2020**, *5* (3), 975−993.
(21) Wu, Z.; Bak, S.-M.; Shadike, Z.; Yu, S.; Hu, E.; Xing, X.; Du, Y.; Yang, X.-Q.; Liu, H.; Liu, P. Understanding the Roles of the Electrode/Electrolyte Interface for Enabling Stable Li||Sulfurized Polyacrylonitrile Batteries. *ACS Appl. Mater. Interfaces* **2021**, *13* (27), 31733−31740.
(22) Chen, J.; Han, K. S.; Henderson, W. A.; Lau, K. C.; Vijayakumar, M.; Dzwiniel, T.; Pan, H.; Curtiss, L. A.; Xiao, J.; Mueller, K. T.; et al. Restricting the Solubility of Polysulfides in Li-S Batteries Via Electrolyte Salt Selection. *Adv. Energy Mater.* **2016**, *6* (11), 1600160.
(23) Huang, C.-J.; Cheng, J.-H.; Su, W.-N.; Partovi-Azar, P.; Kuo, L.-Y.; Tsai, M.-C.; Lin, M.-H.; Panahian Jand, S.; Chan, T.-S.; Wu, N.-L.; et al. Origin of shuttle-free sulfurized polyacrylonitrile in lithium-sulfur batteries. *J. Power Sources* **2021**, *492*, 229508.
(24) Mukkabla, R.; Buchmeiser, M. R. Cathode materials for lithium−sulfur batteries based on sulfur covalently bound to a polymeric backbone. *J. Mater. Chem. A* **2020**, *8* (11), 5379−5394.
(25) Swallow, J. E. N.; Fraser, M. W.; Kneusels, N.-J. H.; Charlton, J. F.; Sole, C. G.; Phelan, C. M. E.; Björklund, E.; Bencok, P.; Escudero, C.; Pérez-Dieste, V.; et al. Revealing solid electrolyte interphase formation through interface-sensitive Operando X-ray absorption spectroscopy. *Nat. Commun.* **2022**, *13*, 6070.
(26) Feng, X.; Song, M. K.; Stolte, W. C.; Gardenghi, D.; Zhang, D.; Sun, X.; Zhu, J.; Cairns, E. J.; Guo, J. Understanding the degradation mechanism of rechargeable lithium/sulfur cells: a comprehensive study of the sulfur-graphene oxide cathode after discharge-charge cycling. *Phys. Chem. Chem. Phys.* **2014**, *16* (32), 16931−16940.
(27) Xiong, S.; Regula, M.; Wang, D.; Song, J. Toward Better Lithium−Sulfur Batteries: Functional Non-aqueous Liquid Electrolytes. *Electrochem. Energy Rev.* **2018**, *1* (3), 388−402.
(28) Liu, Q.; Cresce, A.; Schroeder, M.; Xu, K.; Mu, D.; Wu, B.; Shi, L.; Wu, F. Insight on lithium metal anode interphasial chemistry: Reduction mechanism of cyclic ether solvent and SEI film formation. *Energy Storage Mater.* **2019**, *17*, 366−373.
(29) Kappler, J.; Klostermann, S. V.; Lange, P. L.; Dyballa, M.; Veith, L.; Schleid, T.; Weil, T.; Kästner, J.; Buchmeiser, M. R. Sulfur-Composites Derived from Poly(acrylonitrile) and Poly(vinylacetylene) − A Comparative Study on the Role of Pyridinic and Thioamidic Nitrogen. *Batteries Supercaps* **2023**, *6*, e202200522.
(30) Ahmed, M. S.; Lee, S.; Agostini, M.; Jeong, M.-G.; Jung, H.-G.; Ming, J.; Sun, Y.-K.; Kim, J.; Hwang, J.-Y. Multiscale Understanding of Covalently Fixed Sulfur−Polyacrylonitrile Composite as Advanced Cathode for Metal−Sulfur Batteries. *Adv. Sci.* **2021**, *8* (21), 2101123.
(31) Wang, X.; Qian, Y.; Wang, L.; Yang, H.; Li, H.; Zhao, Y.; Liu, T. Sulfurized Polyacrylonitrile Cathodes with High Compatibility in Both Ether and Carbonate Electrolytes for Ultrastable Lithium−Sulfur Batteries. *Adv. Funct. Mater.* **2019**, *29* (39), 1902929.
(32) Wang, S.; Lu, B.; Cheng, D.; Wu, Z.; Feng, S.; Zhang, M.; Li, W.; Miao, Q.; Patel, M.; Feng, J.; et al. Structural Transformation in a Sulfurized Polymer Cathode to Enable Long-Life Rechargeable Lithium−Sulfur Batteries. *J. Am. Chem. Soc.* **2023**.
(33) Hammersley, A. P.; Svensson, S. O.; Hanfland, M.; Fitch, A. N.; Hausermann, D. Two-dimensional detector software: From real detector to idealised image or two-theta scan. *High Press. Res.* **1996**, *14* (4−6), 235−248.
(34) Qiu, X.; Thompson, J. W.; Billinge, S. J. L. PDFgetX2: a GUI-driven program to obtain the pair distribution function from X-ray powder diffraction data. *J. Appl. Crystallogr.* **2004**, *37* (4), 678.
(35) Ravel, B.; Newville, M. ATHENA, ARTEMIS, HEPHAESTUS: data analysis for X-ray absorption spectroscopy using IFEFFIT. *J. Synchrotron Radiat.* **2005**, *12* (4), 537−541.

https://doi.org/10.1021/acsenergylett.3c00281
ACS Energy Lett. 2023, 8, 2496−2504